RESEARCH ARTICLE OPEN ACCESS

TSPO-Detectable Chronic Active Lesions Predict Disease Progression in Multiple Sclerosis

Eero Polvinen, MD, Markus Matilainen, PhD, Marjo Nylund, MSc, Marcus Sucksdorff, MD, and Laura M. Airas, MD, PhD

Correspondence
Dr. Airas
laura.airas@utu.fi

Neurol Neuroimmunol Neuroinflamm 2023;10:e200133. doi:10.1212/NXI.0000000000200133

Abstract

Background and Objectives

In the multiple sclerosis (MS) brain, chronic active lesions can be detected using MRI- and PET-based methods. In this study, we investigated whether the frequency of TSPO-PET–detectable chronic active lesions associates with disease progression measured using the Expanded Disability Status Scale (EDSS) at 5-year follow-up.

Methods

Chronic lesion–associated innate immune cell activation was evaluated using TSPO-PET in 82 patients with MS. Chronic lesions were categorized into rim-active, inactive, and overall active lesion subtypes based on innate immune cell activation patterns in the lesion core and at the 2-mm perilesional rim. Logistic regression was used to identify best predictors of progression.

Results

Twenty-one patients experienced disability progression during the follow-up. These patients had a significantly higher proportion of rim-active lesions ($p < 0.001$) and a significantly lower proportion of inactive lesions ($p = 0.001$) compared with nonprogressed patients. The results were similar in the patient group having no relapses during the follow-up (60 patients, 14 experienced progression). In logistic regression modeling, the categorized variable "patients with >10% rim-active lesions and ≤50% inactive lesions of all chronic lesions" predicted disease progression in the entire cohort (OR = 26.8, $p < 0.001$) and in the group free of relapses (OR = 34.8, $p = 0.002$).

Discussion

The results show that single TSPO-PET–based in vivo lesion phenotyping of chronic MS lesions provides a strong predictor for MS disease progression. This emphasizes the significance of chronic active lesions in disability accumulation in MS.

From the Turku PET Centre (E.P., M.M., M.N., M.S., L.M.A.); Clinical Neurosciences (E.P., M.N., M.S., L.M.A.), University of Turku; Faculty of Science and Engineering (M.M.), Åbo Akademi University; and Neurocenter (M.S., L.M.A.), Turku University Hospital, Finland.

Go to Neurology.org/NN for full disclosures. Funding information is provided at the end of the article.

The Article Processing Charge was funded by Turku University Hospital, Turku, Finland.

Glossary

AIC = Akaike information criterion; **ARR** = annualized relapse rate; **AUC** = area under the curve; **DMT** = disease-modifying treatment; **DVR** = distribution volume ratio; **EDSS** = Expanded Disability Status Scale; **FLAIR** = fluid-attenuated inversion recovery; **ROI** = region of interest; **RRMS** = relapsing-remitting multiple sclerosis; **SELs** = slowly expanding lesions; **SPMS** = secondary progressive MS.

In most cases, multiple sclerosis (MS) begins as a relapsing-remitting disease (RRMS), but many patients proceed to secondary progression characterized by gradual disability accumulation.[1] In secondary progressive MS (SPMS), trafficking of leukocytes from the periphery into the CNS and formation of focal inflammatory lesions are tuned down. Instead, CNS-contained innate immune cell activation dominates.[2,3] In neuropathologic studies, microglial activation can be observed both diffusively in the normal-appearing white matter and concentrated at the edge of chronic lesions, which demarcates these lesions as chronic active lesions.[4,5] Chronic active lesions are associated with signs of ongoing axonal injury and demyelination.[6,7] They can be detected in vivo using PET imaging and radioligands binding to the 18-kDa translocator protein (TSPO).

Despite the numerous studies[8-12] indicating an association between smoldering inflammation and disability, none of the yet tested imaging markers have been established as a particularly strong predictor for disability accumulation and disease progression in MS. The aim of this study was to evaluate the significance of lesion subtype distribution as a predictor for disease progression. The study focuses on the presence of both chronic active and chronic inactive lesions and was performed using TSPO-PET imaging in a prospective follow-up setting.

Methods

Standard Protocol Approvals, Registrations, and Patient Consents

The study protocol was approved by the Ethics Committee of the Hospital District of Southwest Finland. All participants signed written informed consent, and the study was performed according to the Declaration of Helsinki.

Study Patients

Of the 82 patients with MS included in this study, 59 had RRMS and 23 had SPMS. The patients were recruited from the outpatient clinic of the Division of Clinical Neurosciences at the University Hospital of Turku, Finland. Eligibility criteria were a diagnosis of MS according to McDonald criteria 2017[13] and willingness to participate in a PET study. An additional requirement was a minimum clinical follow-up of 2 years after PET scanning, with an EDSS evaluation at the end of the follow-up. To avoid the effects of acute focal inflammation on innate immune cell activation, exclusion criteria included clinical relapse and/or corticosteroid treatment within 30 days of clinical evaluation and gadolinium contrast enhancement in MRI. In addition, inability to tolerate PET or MRI, current pregnancy, active neurologic or autoimmune disease other than MS, or another significant comorbidity was considered as exclusion criteria. The disease severity and progression were evaluated using the EDSS. EDSS values were evaluated at baseline and at the end of the follow-up. The values were evaluated by experienced clinicians using a standardized examination form, the Neurostatus (neurostatus.net). An EDSS increase of 1.0 point, or 0.5 point if baseline EDSS was ≥6.0, was considered as confirmed disease progression. In all cases, where progression was noted, the EDSS evaluation was confirmed by re-evaluation after 6 months.[14]

MRI Data Acquisition and Analysis

Study patients were scanned with MRI (3T Ingenuity TF PET/MR scanner, Philips or a Gyroscan Intera 1.5T Philips Nova Dual scanner, Philips, Best, the Netherlands) at the time of PET imaging as described before.[15,16] The used MRI sequences were axial T2, 3D fluid-attenuated inversion recovery (FLAIR), 3D T1, and 3D T1 with gadolinium enhancement. The MR images were used for the evaluation of MS lesion pathology and acquisition of anatomic reference for the PET images. Lesional region-of-interest (ROI) masks were created using a semiautomated method as previously described.[15] The Lesion Segmentation Tool (LST) (a toolbox running in SPM8)[17] was used for semiautomated T2 lesion segmentation, and the resulting mask was then manually corrected. The T1 lesion mask was manually edited from the finalized T2 lesion mask, and T1 lesion volumes were obtained from these masks as described previously.[15] The filled T1 image was used for segmenting the gray matter, white matter, and thalamus with FreeSurfer 5.3 software. T1 lesion loads were measured from manually edited T1 lesion ROIs. Lesions ≤27 mm^3 were excluded to avoid inclusion of unspecific T1 hypointensities. The perilesional rim ROI (2 mm) was created by dilating the T1 lesion ROI by 2 voxels from the lesion edge and then removing the T1 lesion ROI. The NAWM ROI was created by removing the T1 lesion ROI and the perilesional rim ROI from the white matter ROI. Because of the limited intrinsic spatial resolution of high-resolution research tomograph (HRRT) PET scanner (resolution 2.5 mm), lesions with less than 75% of the lesion volume in the white matter and lesions with ≤27 mm^3 rim volume or core volume in the white matter were excluded. To avoid potential infratentorial artifacts, lesions in the cerebellum and brain stem were also excluded.

PET Image Acquisition

All TSPO-PET imaging was performed at the Turku PET Centre between 2009 and 2017. The radioligand used in this study was ^{11}C-PK11195, and the radiochemical synthesis

of the ligand was performed as previously described.[15] The injected dose was 480 (±41) MBq, mean (±SD).

PET scan was performed with a brain-dedicated ECAT HRRT scanner (CTI/Siemens) with an intrinsic spatial resolution of 2.5 mm. Attenuation correction was performed using a ^{137}Cs point source in a 6-minute transmission scan. Next, a 60-minute dynamic PET scan was started simultaneously with IV bolus injection of the radioligand. A thermoplastic mask was used to minimize head movements during the scan.

PET Image Postprocessing and Analysis

PET images were reconstructed using 17 time frames as described previously.[15] The dynamic data were then smoothed using a gaussian 2.5-mm postreconstruction filter.[15,18] Possible displacements between frames were corrected using mutual information realignment in SPM8. PET images were coregistered to T1 MR images and resampled to match the MRI voxel size 1 × 1 × 1 mm. Innate immune cell activity and distribution was evaluated as specific binding of radioligand using distribution volume ratio (DVR) in prespecified ROIs. For the estimation of the ^{11}C-PK11195 DVR, the time activity curve corresponding to a reference region devoid of specific TSPO binding was acquired for each PET session using a supervised cluster algorithm with 4 predefined kinetic tissue classes (SuperPK software).[19,20] The reference tissue-input Logan method with a time interval from 20 to 60 minutes was applied to the regional time activity curves using the supervised cluster algorithm gray reference input.

Chronic Lesion Classification Based on TSPO-PET–Measurable Innate Immune Cell Activation

The threshold value for abnormally high voxel activity was calculated as previously described.[12] The threshold was based on the average of 18 healthy controls' mean + 1.96 × SD DVR values of all white matter voxels. The voxels exceeding this DVR value (1.56) were classified as active voxels. Clusters with less than 3 connected voxels were excluded to avoid inclusion of random peak values. The proportions of active voxels in the lesion core ROI and at the rim ROI were used to classify lesions into 3 subtypes as previously described[12]: (1) rim-active lesions: lesions with less than 5% active voxels of all voxels in the lesion core and at least 5%-point higher proportion of active voxels at the rim compared with the core, and lesions with 5%–20% active voxels in the core and at least twice the core activity at the rim; (2) inactive lesions: lesions with no active voxels at the rim or in the core; and (3) overall active lesions: lesions that do not fit into the other 2 categories.

Statistical Analysis

The statistical analysis was performed using R software (version 4.1.1). Variables are presented as median (interquartile range [IQR]), unless otherwise stated. A Wilcoxon rank-sum test was used for comparisons between MS subgroups and in the initial "progression" vs "no progression" comparisons. The associations between continuous variables were assessed using Spearman's rank correlation coefficient.

EDSS change was assessed using logistic regression in the entire patient cohort and in the patient cohort having no relapses during the follow-up. PET-based parameters were of main interest in modeling. These included continuous variables, i.e., the number, proportion, total volume, and proportion of the total volume of rim-active, overall, and inactive lesion types. In addition, proportions of lesion types were analyzed as categorized variables: the proportion of rim-active lesions >10% vs ≤10% (high vs low), the proportion of inactive lesions >35% vs ≤35% (high vs low), and the combination of a high proportion of rim-active lesions (>10%) and a low proportion of inactive lesions (≤50%) vs others. These cutoff percentages were chosen based on visual inspection of the box plots (Figure 1) reporting on the proportion of lesion subtypes in patients with or without progression, with choosing the percentage that seemed to best separate these 2 clinical outcomes. In addition to the variables of main interest, other relevant disease-related variables, such as T1 lesion load, T1 lesion number, brain volume, EDSS at imaging, age, gender, disease duration, the follow-up time, annualized relapse rate (ARR), and disease-modifying treatment (DMT) either within the first 3 years after disease onset or within 2 months of imaging were tested in the modeling. Both DMT variables were categorized into no DMT, moderate efficacy DMT (dimethyl fumarate, fingolimod, glatiramer acetate, interferons, and teriflunomide), and high efficacy DMT (alemtuzumab, natalizumab, ocrelizumab, and rituximab).

The modeling was performed in 2 phases. First, all variables were tested individually using univariate analysis to quantitate the predictive value of each variable. For lesion subtype proportions, T1 lesion load and lesion number, age, and disease duration, the ORs are presented for 10 unit increase to demonstrate significant differences. Similarly, for brain volume, the ORs are presented for 100 cm^3 increase. Logarithm transformations were used in the models for lesion subtype numbers (log(number + 1)) and volumes (log(volume + 1)) to meet the model assumptions. Second, all variables were applied together in forward-type stepwise logistic multivariate regression modeling.[11] In the second phase, the modeling started with a model with no predictors, and new variables were tested one by one. The variable was kept in the model if the model fit compared with the previous model was better according to Akaike information criterion (AIC), and it produced a lower AIC value than any other potential variable. The chosen model was the one with the lowest AIC value. The model assumptions were checked for this model, and finally, the estimated coefficients based on this model were exponentiated to get the ORs. The final combined model from phase 2 was further validated using leave-one-out cross-validation. The receiver operating characteristic curve was estimated, and the area under the curve (AUC) value was calculated. Furthermore, if the probability of progression was at least 50%, the patient was classified as "progression predicted" and otherwise "progression not predicted." The sensitivity and specificity were calculated using this categorization.

All tests were 2-tailed, and p values less than 0.05 were considered as statistically significant for all analyses.

Figure 1 Most Relevant Lesion Subtype Variables in Progressed and Nonprogressed Patients

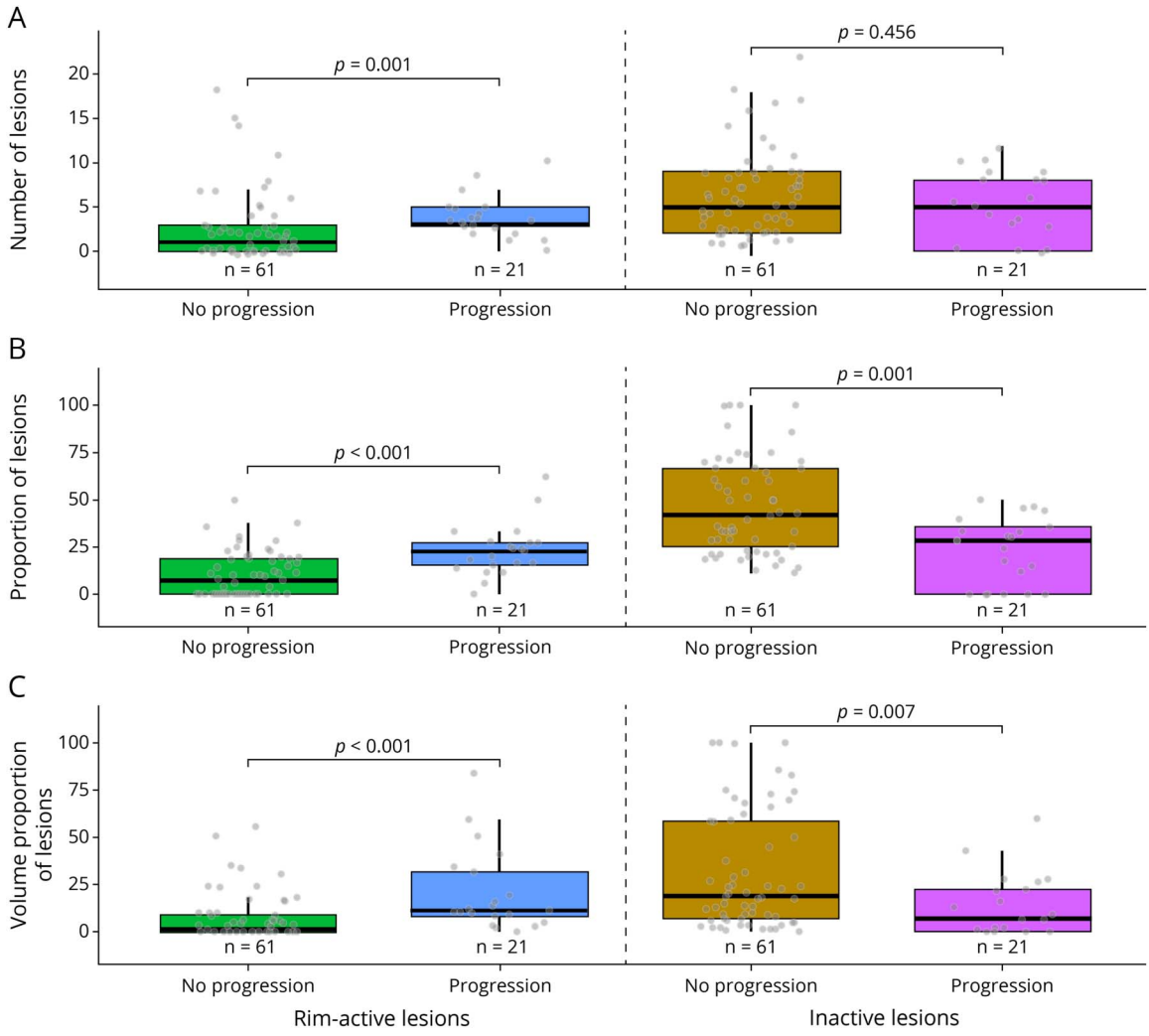

Number of rim-active and inactive lesions (A) and absolute and volume proportions of rim-active and inactive lesions (B and C) in progressed and non-progressed patients with MS in the entire cohort. Progressed patients had a significantly higher number of rim-active lesions and absolute and volume proportions of rim-active lesions compared with nonprogressed patients. Progressed patients had significantly lower absolute and volume proportions of inactive lesions compared with nonprogressed patients.

Data Availability

Anonymized data not published within the article will be shared over the next 3 years on request from a qualified investigator.

Results

Demographic, Clinical, and Imaging Characteristics of the Participants

Of the 82 patients included in this study, 18 (22%) were males, and 64 (78%) were females. The mean age was 45.7 (±9.3) years, (±SD) and disease duration was 13.1 (±7.7) years. At baseline, the EDSS score was 3 [2–4] (median [IQR]), and the ARR during the entire disease history before PET imaging was 0.32 [0.22–0.47]. The mean follow-up time after PET imaging was 5.0 years (±1.7; SD). Fifty-nine of the patients were classified as patients with RRMS, and 23 had SPMS. TSPO binding (DVR) was statistically significantly higher within the NAWM of patients with SPMS compared with patients with RRMS ($p < 0.001$), but not in the thalamus or in the perilesional area (eFigure 1, links.lww.com/NXI/A870). Twenty-one patients (26%) experienced disease progression during the follow-up. Of them, 10 had RRMS, and 11 had SPMS, and 14 were relapse free during the follow-up. No differences were observed at baseline in T1 lesion load, brain volume, NAWM volume, thalamus volume, or cortical gray matter volume in progressed vs nonprogressed patients (Table 1).

Quantification of Chronic Lesion Subtypes Based on TSPO Binding

In the entire 82 patient cohort, the average number of chronic lesions was 13 per patient [7–24] (median [IQR]). Each patient had an average of 2 [0–4] rim-active lesions and an average of 5 [2–9] inactive lesions, whereas the average number of overall active lesions was 6 [3–12] (Table 2). The maximum number of rim-active lesions in an individual

Table 1 Baseline Demographic and Imaging Characteristics of the Cohort

Variable	All patients	Nonprogressed	Progressed	Progressed vs nonprogressed: *p* Value	Follow-up relapse free	Relapse free: nonprogressed	Relapse free: progressed	Relapse free: progressed vs nonprogressed: *p* Value
n	82	61	21		60	46	14	
Females, n (%)	64 (78)	49 (80)	15 (71)	0.5	44 (73)	36 (78)	8 (57)	0.17
Age, y	45.7 (9.3)	45.5 (9.2)	46.4 (9.9)	0.8	45.3 (8.2)	45.4 (8.2)	44.6 (8.5)	0.9
Disease duration, y	13.1 (7.7)	12.6 (8.0)	14.7 (6.6)	0.10	12.7 (7.3)	12.1 (7.1)	14.7 (6.5)	0.093
EDSS at baseline, median (IQR)	3 (2–4)	3 (2–3.5)	3.5 (2.5–6)	0.13	3 (2–4)	2.75 (2–3.5)	3.5 (2.5–6.4)	0.17
T_1 lesion load (cm^3), median (IQR)[a]	3.00 (1.44–8.56)	2.68 (1.10–7.58)	4.23 (2.28–11.3)	0.12	3.07 (1.61–10.7)	3.00 (1.60–8.25)	3.38 (1.75–12.9)	0.5
No. of T1 lesions (>27 mm^3) per patient, median (IQR)[a]	18 (8–31)	13 (7–31)	26 (18–30)	0.091	19 (9–31)	14.5 (9–31)	21 (13.5–29.5)	0.4
NAWM volume (PF)	0.33 (0.036)	0.33 (0.033)	0.33 (0.044)	0.9	0.33 (0.036)	0.32 (0.034)	0.34 (0.040)	0.5
Cortical gray matter volume (PF)	0.31 (0.025)	0.31 (0.021)	0.31 (0.034)	0.4	0.31 (0.022)	0.32 (0.020)	0.31 (0.029)	0.3
Thalamus volume (PF)	0.010 (0.0013)	0.010 (0.0012)	0.010 (0.0015)	0.9	0.010 (0.0013)	0.010 (0.0012)	0.010 (0.0015)	0.7
Whole-brain volume (cm^3)	1,132 (106)	1,144 (97)	1,100 (126)	0.2	1,135 (103)	1,136 (96)	1,120 (127)	0.7
Follow-up duration (y)	5.0 (1.7)	4.9 (1.6)	5.4 (2.0)	0.3	4.9 (1.7)	4.8 (1.6)	5.2 (2.1)	0.5
ARR before baseline, median (IQR)	0.32 (0.22–0.47)	0.32 (0.23–0.46)	0.30 (0.16–0.48)	0.6	0.30 (0.22–0.45)	0.30 (0.22–0.45)	0.29 (0.17–0.44)	0.7
DMT at baseline, n (%)								
No DMT	29 (35)	17 (28)	12 (57)	0.065	21 (35)	12 (36)	9 (64)	**0.038**
Moderate efficacy DMT	43 (52)	35 (57)	8 (38)		32 (53)	28 (61)	4 (29)	
High efficacy DMT	10 (12)	9 (15)	1 (5)		7 (12)	6 (13)	1 (7)	

Abbreviations: ARR = annualized relapse rate; DMT = disease-modifying treatment; EDSS = Expanded Disability Status Scale; IQR = interquartile range; NAWM = normal-appearing white matter; PF = parenchymal fraction. Shown are mean (±SD) values, unless stated otherwise. A Fisher exact test was used to compare proportions of genders (male and female) and to explore similarities of DMT type distributions in progressed vs nonprogressed groups. Here, $p < 0.05$ reports on dissimilarity. Other comparisons are based on the Wilcoxon rank-sum test. The p value indicating a statistically significant difference is bolded.

[a] Including lesions extending to gray matter and infratentorial brain areas.

Table 2 T1 White Matter Lesion Subtypes in MS Patient Subgroups According to Relapse Status and Progression Status During Follow-up

	All patients	No progression during follow-up	Progression during follow-up	No prog. vs prog.: *p* Value	Relapse free	Relapse free: no progression during follow-up	Relapse free: progression during follow-up	Relapse free: no prog. vs prog.: *p* Value
n	82	61	21		60	46	14	
No. of patients with rim-active lesions, n (%)	54 (66)	34 (56)	20 (95)		42 (70)	28 (61)	14 (100)	
No. of patients with inactive lesions, n (%)	76 (93)	61 (100)	15 (71)		55 (92)	46 (100)	9 (64)	
No. of patients with overall active lesions, n (%)	78 (95)	57 (93)	21 (100)		58 (97)	44 (96)	14 (100)	
No. of all chronic lesions	13 (7–24)	11 (7–24)	20 (11–24)	0.13	16 (8–23)	13 (7–24)	19 (13–23)	0.4
No. of rim-active lesions	2 (0–4)	1 (0–3)	3 (3–5)	**0.001**	2 (0–4)	2 (0–3)	4 (2–5)	**0.010**
No. of inactive lesions	5 (2–9)	5 (2–9)	5 (0–8)	0.5	6 (2–9)	6 (3–9)	5 (0–8)	0.2
No. of overall active lesions	6 (3–12)	5 (2–11)	10 (6–13)	**0.040**	7 (3–11)	6 (2–11)	10 (5–14)	0.18
Volume of all lesions (cm^3)	2.26 (0.96–7.49)	2.17 (0.74–6.96)	3.43 (1.86–11.05)	0.13	2.23 (1.04–8.56)	2.23 (0.96–7.49)	2.33 (1.46–11.80)	0.5
Volume of rim-active lesions (cm^3)	0.14 (0–0.45)	0.06 (0–0.36)	0.30 (0.17–1.12)	**0.002**	0.15 (0–0.51)	0.13 (0–0.40)	0.27 (0.12–1.22)	**0.029**
Volume of inactive lesions (cm^3)	0.42 (0.14–0.74)	0.41 (0.16–0.83)	0.44 (0–0.63)	0.3	0.44 (0.14–0.74)	0.44 (0.18–0.83)	0.32 (0–0.70)	0.2
Volume of overall active lesions (cm^3)	1.55 (0.27–6.11)	1.35 (0.22–5.62)	2.48 (1.07–9.02)	0.11	1.45 (0.37–7.33)	1.39 (0.38–5.74)	1.55 (0.43–9.93)	0.4
Proportion of rim-active lesions (%)[a]	12 (0–23)	7 (0–19)	23 (15–27)	**<0.001**	12 (0–20)	10 (0–19)	22 (16–32)	**0.001**
Proportion of inactive lesions (%)[a]	33 (21–57)	42 (25–67)	29 (0–36)	**0.001**	34 (21–58)	41 (23–65)	21 (0–35)	**0.002**
Proportion of overall active lesions (%)[a]	49 (34–60)	46 (29–59)	51 (42–67)	0.060	50 (33–61)	47 (26–59)	52 (42–67)	0.097
Volume proportion of rim-active lesions (%)[a]	5 (0–13)	2 (0–9)	11 (8–31)	**<0.001**	5 (0–16)	3 (0–10)	14 (6–34)	**0.001**
Volume proportion of inactive lesions (%)[a]	17 (5–41)	19 (7–59)	7 (0–22)	**0.007**	14 (3–43)	17 (5–56)	4 (0–25)	**0.026**
Volume proportion of overall active lesions (%)[a]	73 (42–84)	74 (38–85)	69 (59–80)	1	70 (43–85)	74 (42–87)	65 (50–78)	0.6

Shown are median (interquartile range [IQR]) values. The shown *p* values are based on the Wilcoxon rank-sum test. After this, we performed false discovery rate correction. *p* Values indicating statistically significant differences (<0.05) after correction are bolded.
[a] Out of all chronic lesions.

Figure 2 Mean Absolute and Volume Proportions of Lesion Subtypes in Progressed and Nonprogressed Patients

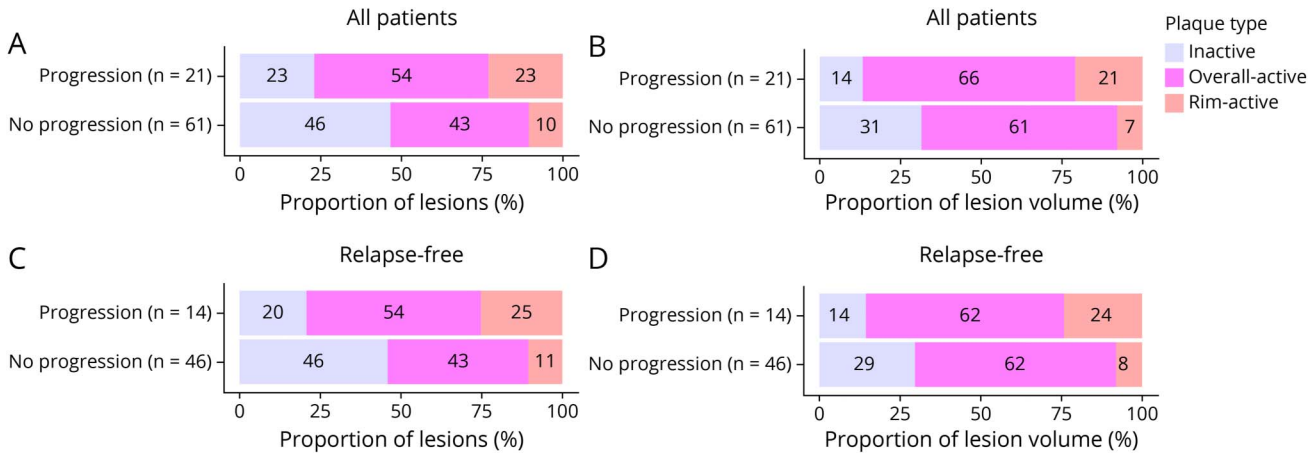

The proportions were significantly different both in the entire cohort (Fisher exact test, $p < 0.001$; A and B) and among patients free of relapses during the follow-up ($p < 0.001$; C and D).

patient was 18. A majority (54; 66%) of patients in the entire cohort had rim-active lesions. These patients had also a higher EDSS and a lower brain volume compared with patients with no rim-active lesions (eFigure 2, links.lww.com/NXI/A870). When we divided the cohort into 2 groups based on median disease duration (12 years), in the group with shorter disease duration, 21 of 41 patients (51%) had rim-active lesions, whereas in the group with longer disease duration, 33 of 41 patients (80%) had rim-active lesions ($p = 0.01$, Fisher test).

The average proportion of rim-active lesions of all chronic lesions was 12 [0–23]%, and the average proportion of inactive lesions was 33 [21–57]%, whereas the average proportion of overall active lesions was 49 [34–60]%. On average, the rim-active lesion volume comprised 5 [0–13]% of the entire lesion volume (volume proportion), whereas the average volume proportions of inactive and overall active lesions were 17 [5–41]% and 73 [42–84]%. The data regarding lesion quantification are shown in Table 2.

Lesion Subtypes Are Differently Distributed in Patients With Progression vs Without Progression

Although there was no difference in the total number of chronic lesions between those patients experiencing progression during the follow-up and patients without progression, the number of rim-active lesions was higher among progressed vs stable patients (3 [3–5] vs 1 [0–3], median [IQR], $p = 0.001$; Figure 1A). Similarly, both the median proportion and median volume proportion of rim-active lesions of all chronic lesions were significantly higher in progressed patients compared with stable patients (23 [15–27]% vs 7 [0–19]% and 11 [8–31]% vs 2 [0–9]%, respectively, $p < 0.001$ for both; Figure 1, B and C). On the other hand, both the proportion and the volume proportion of inactive lesions were lower in progressed patients compared with stable patients (29 [0–36]% vs 42 [25–67]%, $p = 0.001$ and 7 [0–22]% vs 19 [7–59]%, $p = 0.007$; Figure 1, B and C), although no statistically significant difference was observed in the median number of inactive lesions in progressed vs nonprogressed patients. The prevalence and volume of overall active lesions were mostly similar in progressed vs nonprogressed patients (Figure 2). The only exception here was that progressed patients had a slightly higher number of overall active lesions compared with nonprogressed patients ($p = 0.040$). All rim-active and inactive plaque-type–related parameters correlated significantly with later EDSS change (eFigure 3, links.lww.com/NXI/A870). The numerical data are shown in Table 2.

Results regarding lesion subtypes and later progression were similar to the above-described ones when analyzed within the group of patients experiencing no relapses during the follow-up, with similar statistically significant associations with EDSS change (Table 2).

Lesion subtypes also differed in patients with RRMS vs SPMS. The proportion of rim-active lesions was significantly higher in SPMS compared with RRMS (18% vs 10%, $p = 0.018$). The proportion of inactive lesions was, on the other hand, higher among RRMS compared with SPMS (36% vs 24%, $p = 0.014$), but there was no statistically significant difference in the proportion of overall active lesions between RRMS and SPMS (47% vs 53%, $p = 0.06$, eTable 1, links.lww.com/NXI/A870).

Prediction of Disease Progression Using Lesion Subtype Distribution and Other Imaging and Clinical Variables

First, univariate logistic regression modeling was performed separately for each individual PET parameter and other relevant disease-related clinical and imaging variables to test their ability to predict later disease progression. Some

Figure 3 Forest Plot Demonstrating Results From Modeling of Progression in the Entire Cohort

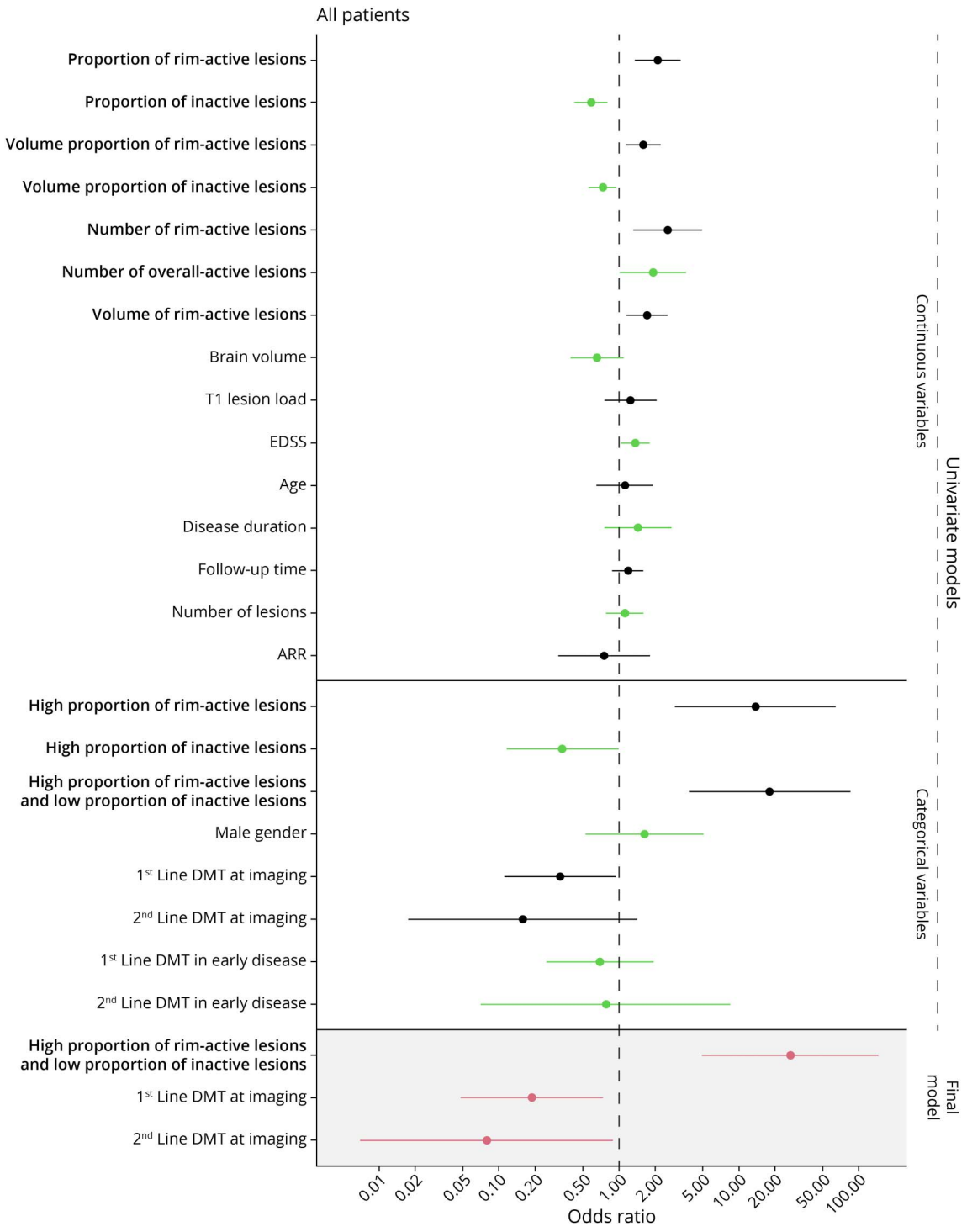

First, univariate logistic regression models were used separately for each individual PET-parameter and other relevant disease-related clinical and imaging variables. All significant PET-related predictors are displayed. In addition, all non–PET-related variables are shown. Only PET-related parameters and treatment type at imaging were found to be statistically significant in predicting progression as individual parameters both in the entire patient cohort and in the cohort with no relapses during the follow-up (eFigure 4, links.lww.com/NXI/A870). In addition, the EDSS at imaging was a significant predictor in the entire patient cohort. The final model, marked with gray background, was obtained using forward-type stepwise multivariate logistic regression for the entire patient cohort. All variables for which the univariate model is presented were tested in the multivariate model. The addition of each variable to the final model was determined using Akaike information criterion (AIC). The new variable remained in the final model if it lowered the AIC value. The chosen final model was the combination of variables that produced the lowest AIC value. Dots are ORs, and lines around them represent the 95% CIs. If the lines do not cross the dashed line marking OR = 1, the result is statistically significant. ARR = annualized relapse rate; DMT = disease-modifying treatment; EDSS = Expanded Disability Status Scale.

PET-related parameters and the treatment type at imaging were found to be statistically significant in predicting progression as individual parameters both in the entire patient cohort (Figure 3) and in the cohort with no relapses during the follow-up (eFigure 4, links.lww.com/NXI/A870). In addition, the EDSS at imaging was a significant predictor in the entire patient cohort (Figure 3).

Stepwise logistic regression modeling was then performed to include several variables simultaneously to build the best multivariate model. All variables that lowered the AIC value remained in the final model as predictors for disease progression. In both groups (i.e., the entire cohort and the patient group with no relapses during the follow-up), the best predictors for disease progression were (1) a combined categorized variable: "a high proportion of rim-active lesions and a low proportion of inactive lesions vs others" and (2) the type of DMT within 2 months of PET imaging (no DMT, moderate efficacy DMT, or high efficacy DMT). In this model, the combined lesion variable predicted disease progression in the entire patient cohort with OR = 26.8, $p < 0.001$, whereas a DMT at baseline reduced the odds of disease progression (Figure 3 and Table 3).

In the final model for the patient group free of relapses, the combined lesion variable predicted disease progression with OR = 34.8, $p = 0.002$, and DMT at baseline reduced the odds of disease progression (Table 3 and eFigure 4, links.lww.com/NXI/A870).

In the entire patient cohort, the final model predicted disease progression with 57% sensitivity and 97% specificity, with an AUC value of 0.76. In the patient group free of relapses, the model predicted progression with 64% sensitivity and 96% specificity, with an AUC value of 0.75 (Figure 4).

Of interest, the final model produced progression probabilities to all patients belonging to one of these groups. For example, in the entire cohort, patients who belonged to group "no DMT at baseline" and "a high proportion of rim-active lesions and a low proportion of inactive lesions" had 75% chance of disease progression during the follow-up according to the model. For comparison, patients in the group "moderate efficacy DMT" and "a high proportion of rim-active lesions and a low proportion of inactive lesions" had 36% chance of disease progression. The disease progression probabilities in the entire cohort and in the patient group free of relapses are shown in Table 3.

We also tested a multivariate model where we omitted PET-related data and only included demographic factors, conventional MRI parameters, and the type and timing of treatment as predictors, but this model failed to detect progressors among the present cohort.

Discussion

This prospective study of 82 patients with MS elucidates the risk of disability worsening by using information from TSPO-PET imaging for chronic lesion–related brain innate immune cell activation. Stepwise logistic regression modeling showed that patients with MS who had a combination of abundant chronic active lesions and a low proportion of chronic inactive lesions were most likely to experience later progression during a 5-year follow-up. When untreated, such patients had a progression probability of 75%, whereas for patients with other lesion type combinations, the progression probability was only 10% during a 5-year follow-up. These results support the notion that smoldering lesion-associated inflammation contributes to disability-promoting pathology,[10,21,22] whereas

Table 3 Associations Between the Best Predictors and EDSS Progression in All Patients With MS and in a Subgroup of Patients Who Were Relapse Free During the Follow-up

	Stepwise logistic regression					
	All patients (n = 82)			Patients with no relapses (n = 60)		
Predictors in the model	Estimate	OR	*p* Value	Estimate	OR	*p* Value
High rim-active and low inactive proportion of lesions[a]	3.29	26.8	<0.001	3.55	34.8	0.002
Moderate efficacy DMT at imaging	−1.67	0.19	0.017	−2.07	0.13	0.017
High efficacy DMT at imaging	−2.54	0.08	0.041	−2.22	0.11	0.092
Progression probabilities (%) based on the model	**No DMT**	**Moderate efficacy DMT**	**High efficacy DMT**	**No DMT**	**Moderate efficacy DMT**	**High efficacy DMT**
Patients with high rim-active and low inactive proportions	75.0	35.9	19.1	74.7	27.2	24.3
Other patients	10.0	2.0	0.9	7.8	1.1	0.9

Abbreviations: DMT = disease-modifying treatment; EDSS = Expanded Disability Status Scale.
Progression was modeled using forward-type stepwise logistic regression as described in Statistical Analysis. Here, testing started with no variables in the model, and the addition of each PET-related, clinical, and MRI variable was tested using the Akaike information criterion. The individual variables are listed in Statistical analysis. Estimates are logarithmic ORs.
[a] Patients with >10% rim-active lesions and ≤50% inactive lesions.

Figure 4 Receiver Operating Characteristic Curves With AUC Values

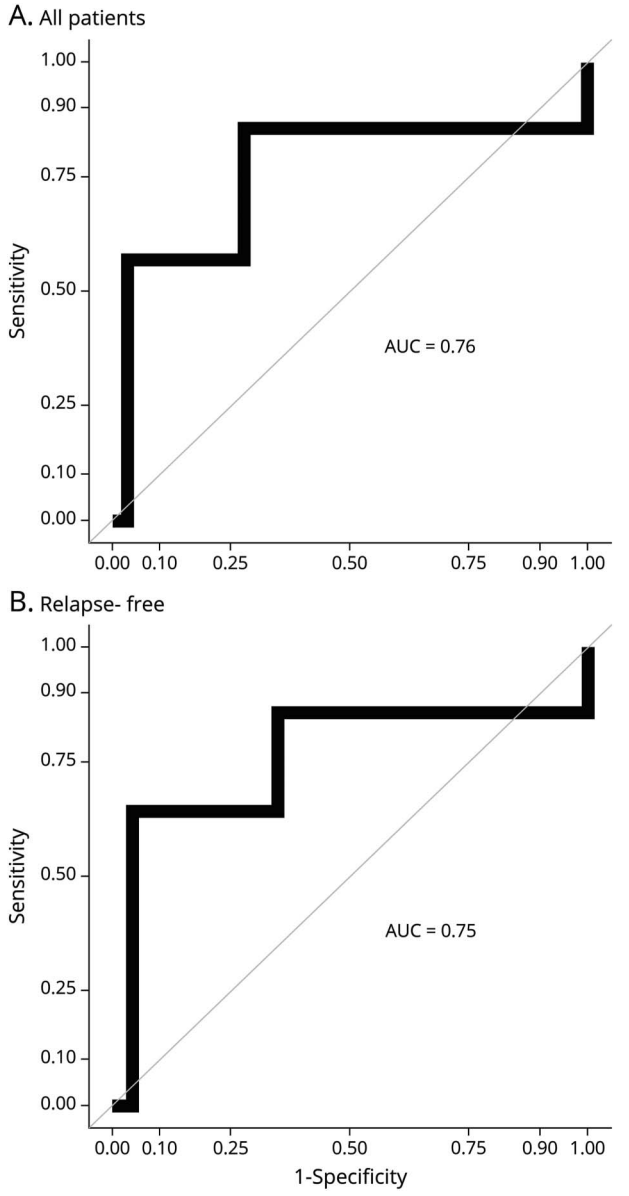

In the entire cohort (A), the logistic regression model predicted correctly progression in 12 of 21 patients (sensitivity = 57%) and no progression in 59 of 61 patients (specificity = 97%). In the patient group free of relapses (B), the model predicted correctly progression in 9 of 14 patients (sensitivity = 64%) and no progression in 44 of 46 patients (specificity = 96%). AUC = area under the curve.

a remarkable share of the chronic lesions, i.e., those with no prominent rim activity, seems to have a less significant role in driving MS progression. This is in line with previous cross-sectional studies that have shown an association between a higher number of iron rim+ lesions and a higher degree of cognitive and motor disability in MS.[8] However, in another study, no difference in the presence of iron rim lesions was observed when patients were categorized according to clinical MS subtype, gender, disease duration, treatment, or EDSS.[23] Our earlier TSPO-PET–based study reported that high perilesional TSPO binding in the normal-appearing white matter predicted disease progression in MS.[11] In this study, the perilesional area was defined as a relatively large combined area, extending 6 voxels deep into the normal-appearing white matter collectively from the edge of the lesions. No comparisons in binding activity were performed between the perilesional area and the lesion core or between individual lesions.[11]

Progression independent of relapses can take place at any stage of the disease and expedite disability accrual in situations where relapses and new focal MRI activity are kept under control using efficient anti-inflammatory therapies.[24] In our study, 59 patients had RRMS, and 23 had SPMS. Of the 21 progressors, nearly half (48%) were classified as having RRMS, and the majority of these patients with RRMS (80%) were still on DMT at the time of imaging. Of the patients with RRMS, 35 (59%) had TSPO rim-active lesions. This is in line with the previously published studies demonstrating iron rim+ lesions at all stages of MS.[21] In our study, most patients in the entire cohort had rim-active lesions, and these patients had a higher EDSS and a lower brain volume compared with patients with no rim-active lesions. In addition, more patients had rim-active lesions in the patient group with longer disease duration compared with shorter disease duration. This conforms well with the higher likelihood of clinical progression in more advanced disease. Based on the known tendency of the chronic active lesions to grow with time, specific algorithms have been developed to quantitate slowly expanding lesions (SELs) in an automated fashion from conventional MR images.[25] SELs were identified more frequently in patients with primary progressive MS (PPMS) compared with patients with RRMS, and it was hypothesized that SELs may represent a conventional brain MRI correlate of chronic active lesions.[25] Notably, in a recent study, SELs were also associated with later disease progression.[26]

Overall, 43% of all progressors were on treatment at imaging, and it was noted based on logistic regression modeling that besides the proportion of TSPO-rim-positive lesions, also MS treatment at the time of imaging significantly affected later disease progression, similarly as has been shown previously in large real-world studies particularly at early stages of the disease.[27,28] This suggests that the progression-promoting innate immune cell activation is linked to the activity of the peripherally driven adaptive immune system. According to our model, the utilization of (mostly peripherally acting) DMTs reduced progression probability from 74.7% to 27.2% in the cohort with the highest risk of progression based on the presence of TSPO-PET-demonstrable rim-active lesions. In line with this, a larger proportion of the progressors (57%) had no DMT compared with the entire cohort (35%).

Our study confirms that the number and the volume of chronic active lesions associate strongly with later disease progression and thus corroborate the adverse role of TSPO-PET-measurable innate immune cell activation at the chronic

lesion edge in MS. On the other hand, our work also demonstrates the more benign nature of inactive chronic lesions. Of the 82 patients, 28 (34%) had no TSPO-rim-positive chronic active lesions. These patients had a higher proportion of chronic inactive (TSPO-rim-negative) lesions, and all but one of these patients (96%) were clinically stable. Of the patients experiencing progression during the 5-year follow-up, all but one had chronic active lesions, with an average of 3 lesions per patient (range 0–10). On the other hand, 27 of the 61 (44%) patients with no progression had no chronic active lesions. Finally, a high proportion of TSPO-rim-positive lesions combined with a low proportion of TSPO-rim-negative lesions remained as a significant predictor in the logistical regression analysis even when considering relevant confounding factors, such as EDSS, treatment, lesion load, age, and disease duration. Our results suggest that chronic lesion subtyping provides a good prognostic marker for later disease progression. Treatment type failed to predict progression independently, but in the multivariate regression model it remained as a significant predictor. In earlier studies, several factors, including demographic variables (baseline EDSS, age, gender, and disease activity), MRI parameters (brain atrophy, T2 lesion load, baseline gadolinium-enhancing lesion load, spinal lesions, and cortical lesions), and type of treatment, have been shown to associate with later disease progression.[29-32] The significance of these variables has been shown to be particularly strong when measured in the early stages of the disease.[29-31] We tested several relevant non–PET-related variables in the univariate model, but most of these were not statistically significant in predicting progression. This discrepancy may be due to the relatively small number of patients included in the current study.

There are some limitations to our study. The definitions for chronic lesion subtyping were based on our recent article.[12] We are aware that methods for chronic lesion phenotyping vary between studies,[33,34] which may create a challenge when comparing results from different studies. The approach we used matches well with lesion phenotyping results from neuropathologic studies, which is reassuring regarding the applicability of our method.[5] Accordingly, patients with SPMS had a significantly larger proportion of rim-active lesions and a smaller proportion of inactive lesions compared with patients with RRMS.[12] A significant proportion (49%) of all chronic lesions were classified as overall active lesions, with TSPO binding both at the rim and in the core. Also, previous cross-sectional PET studies have reported significant TSPO binding in the core of chronic lesions,[35,36] but the exact nature of this lesion subtype remains somewhat elusive.[37,38] In this study, the overall active lesions were considered as an exclusionary lesion category based on their indefinite role in predicting disease progression. Furthermore, only supratentorial white matter lesions were included in this study, whereas infratentorial, spinal, and gray matter lesions may also contribute critically to disability and have an effect on disease progression.[31,39] Another limitation of our study was the lack of longitudinal MRI. Hence, although the patients did not experience relapses during the follow-up, we cannot be entirely certain that the disease worsening during the follow-up was not related to new focal inflammatory activity.

Understanding the pathology behind interindividual differences in disability accrual improves the odds of successful development of new treatments to prevent disease progression. Screening for patients with TSPO-rim-active lesions to enrich patient populations for progression-targeting treatment trials will likely improve chances of therapeutic success. On the other hand, lack of microglial activation at chronic lesion rim associates with low progression risk, and our results may hence later benefit clinicians who need to make a choice which patients to treat with progression-halting medications. Similar decision-making aids based on risk modeling are already in clinical use in other diseases, such the CHA(2)DS(2)-VASc for evaluating the need of anticoagulation treatment for atrial fibrillation.[40] For MS, specific blood-measurable biomarkers correlating with TSPO-PET findings will be of uttermost significance here.

Although it is not these days commonplace to use TSPO-PET imaging for the evaluation of MS brain pathology in the clinical setting, we do not see this as an impossible scenario in the future. A good comparative example is Alzheimer disease, where a preceding PET image with demonstration of amyloid deposition is recommended before the initiation of immune treatment with aducanumab.[41] In addition, the development of automated MRI-based iron rim detection and identification of blood-detectable biomarkers associating with smoldering inflammation in the brain may prove useful for providing high-quality individualized care for patients with MS. Despite existing preliminary data demonstrating colocalization of iron rim lesions and TSPO binding,[42] it is yet to be demonstrated how SEL identification, MRI-based iron rim detection, and TSPO-PET imaging methods perform in detecting chronic active lesions when compared with each other head to head at a large scale, or whether their complimentary use will improve the sensitivity of predicting MS progression.

Acknowledgment

The authors thank all people with MS participating in this study and the expert personnel of the Turku PET Centre.

Study Funding

The Academy of Finland (decision number: 330902), the Sigrid Juselius Foundation, the Finnish MS Foundation, the Finnish Medical Foundation, and the InFLAMES Flagship Programme of the Academy of Finland (decision number: 337530).

Disclosure

The authors report no competing interests relevant to this study. E. Polvinen, M. Matilainen, and M. Nylund report no disclosures; M. Sucksdorff has received research support from the Finnish Medical Foundation, the Finnish MS Foundation, and the Finnish Medical Society (Finska Läkaresällskapet); L.

Airas has received honoraria from F. Hoffmann-La Roche Ltd., Genzyme, Janssen, and Merck Serono and institutional research grant support from Academy of Finland, Genzyme, Merck Serono, and Novartis. Go to Neurology.org/NN for full disclosure.

Publication History

Received by *Neurology: Neuroimmunology & Neuroinflammation* October 9, 2022. Accepted in final form April 21, 2023. Submitted and externally peer reviewed. The handling editor was Associate Editor Friedemann Paul, MD.

Appendix Authors

Name	Location	Contribution
Eero Polvinen, MD	Turku PET Centre; Clinical Neurosciences, University of Turku, Finland	Drafting/revision of the manuscript for content, including medical writing for content, and analysis or interpretation of data
Markus Matilainen, PhD	Turku PET Centre; Faculty of Science and Engineering, Åbo Akademi University, Finland	Drafting/revision of the manuscript for content, including medical writing for content, and analysis or interpretation of data
Marjo Nylund, MSc	Turku PET Centre; Clinical Neurosciences, University of Turku, Finland	Drafting/revision of the manuscript for content, including medical writing for content
Marcus Sucksdorff, MD	Turku PET Centre; Clinical Neurosciences, University of Turku; Neurocenter, Turku University Hospital, Finland	Drafting/revision of the manuscript for content, including medical writing for content; major role in the acquisition of data; and study concept or design
Laura M. Airas, MD, PhD	Turku PET Centre; Clinical Neurosciences, University of Turku; Neurocenter, Turku University Hospital, Finland	Drafting/revision of the manuscript for content, including medical writing for content; major role in the acquisition of data; study concept or design; and analysis or interpretation of data

References

1. Correale J, Gaitán MI, Ysrraelit MC, Fiol MP. Progressive multiple sclerosis: from pathogenic mechanisms to treatment. *Brain*. 2017;140(3):527-546. doi:10.1093/brain/aww258
2. Baecher-Allan C, Kaskow BJ, Weiner HL. Multiple sclerosis: mechanisms and immunotherapy. *Neuron*. 2018;97(4):742-768. doi:10.1016/j.neuron.2018.01.021
3. Lassmann H. Mechanisms of white matter damage in multiple sclerosis. *Glia*. 2014;62(11):1816-1830. doi:10.1002/glia.22597
4. Allen IV, McQuaid S, Mirakhur M, Nevin G. Pathological abnormalities in the normal-appearing white matter in multiple sclerosis. *Neurol Sci*. 2001;22(2):141-144. doi:10.1007/s100720170012
5. Frischer JM, Weigand SD, Guo Y, et al. Clinical and pathological insights into the dynamic nature of the white matter multiple sclerosis plaque. *Ann Neurol*. 2015;78(5):710-721. doi:10.1002/ana.24497
6. Frischer JM, Bramow S, Dal-Bianco A, et al. The relation between inflammation and neurodegeneration in multiple sclerosis brains. *Brain*. 2009;132(Pt 5):1175-1189. doi:10.1093/brain/awp070
7. Prineas JW, Kwon EE, Cho ES, et al. Immunopathology of secondary-progressive multiple sclerosis. *Ann Neurol*. 2001;50(5):646-657. doi:10.1002/ana.1255
8. Absinta M, Sati P, Masuzzo F, et al. Association of chronic active multiple sclerosis lesions with disability in vivo. *JAMA Neurol*. 2019;76(12):1474-1483. doi:10.1001/jamaneurol.2019.2399
9. Beynon V, George IC, Elliott C, et al. Chronic lesion activity and disability progression in secondary progressive multiple sclerosis. *BMJ Neurol Open*. 2022;4(1):e000240. doi:10.1136/bmjno-2021-000240
10. Elliott C, Belachew S, Wolinsky JS, et al. Chronic white matter lesion activity predicts clinical progression in primary progressive multiple sclerosis. *Brain*. 2019;142(9):2787-2799. doi:10.1093/brain/awz212
11. Sucksdorff M, Matilainen M, Tuisku J, et al. Brain TSPO-PET predicts later disease progression independent of relapses in multiple sclerosis. *Brain*. 2020;143(11):3318-3330. doi:10.1093/brain/awaa275
12. Nylund M, Sucksdorff M, Matilainen M, Polvinen E, Tuisku J, Airas L. Phenotyping of multiple sclerosis lesions according to innate immune cell activation using 18 kDa translocator protein-PET. *Brain Commun*. 2022;4(1):fcab301. doi:10.1093/braincomms/fcab301
13. Thompson AJ, Banwell BL, Barkhof F, et al. Diagnosis of multiple sclerosis: 2017 revisions of the McDonald criteria. *Lancet Neurol*. 2018;17(2):162-173. doi:10.1016/S1474-4422(17)30470-2
14. Kalincik T, Cutter G, Spelman T, et al. Defining reliable disability outcomes in multiple sclerosis. *Brain*. 2015;138(Pt 11):3287-3298. doi:10.1093/brain/awv258
15. Rissanen E, Tuisku J, Vahlberg T, et al. Microglial activation, white matter tract damage, and disability in MS. *Neurol Neuroimmunol Neuroinflamm*. 2018;5(3):e443. doi:10.1212/NXI.0000000000000443
16. Bezukladova S, Tuisku J, Matilainen M, et al. Insights into disseminated MS brain pathology with multimodal diffusion tensor and PET imaging. *Neurol Neuroimmunol Neuroinflamm*. 2020;7(3):e691. doi:10.1212/NXI.0000000000000691
17. Schmidt P, Gaser C, Arsic M, et al. An automated tool for detection of FLAIR-hyperintense white-matter lesions in multiple sclerosis. *Neuroimage*. 2012;59(4):3774–3783. doi:10.1016/j.neuroimage.2011.11.032
18. Rissanen E, Tuisku J, Rokka J, et al. In vivo detection of diffuse inflammation in secondary progressive multiple sclerosis using PET imaging and the radioligand ^{11}C-PK11195. *J Nucl Med*. 2014;55(6):939-944. doi:10.2967/jnumed.113.131698
19. Turkheimer FE, Edison P, Pavese N, et al. Reference and target region modeling of [11C]-(R)-PK11195 brain studies. *J Nucl Med*. 2007;48(1):158-167.
20. Yaqub M, van Berckel BN, Schuitemaker A, et al. Optimization of supervised cluster analysis for extracting reference tissue input curves in (R)-[(11)C]PK11195 brain PET studies. *J Cereb Blood Flow Metab*. 2012;32(8):1600-1608. doi:10.1038/jcbfm.2012.59
21. Dal-Bianco A, Grabner G, Kronnerwetter C, et al. Long-term evolution of multiple sclerosis iron rim lesions in 7 T MRI. *Brain*. 2021;144(3):833-847. doi:10.1093/brain/awaa436
22. Giovannoni G, Popescu V, Wuerfel J, et al. Smouldering multiple sclerosis: the real MS. *Ther Adv Neurol Disord*. 2022;15:17562864211066751. doi:10.1177/17562864211066751
23. Treaba CA, Conti A, Klawiter EC, et al. Cortical and phase rim lesions on 7 T MRI as markers of multiple sclerosis disease progression. *Brain Commun*. 2021;3(3):fcab134. doi:10.1093/braincomms/fcab134
24. Kappos L, Wolinsky JS, Giovannoni G, et al. Contribution of relapse-independent progression vs relapse-associated worsening to overall confirmed disability accumulation in typical relapsing multiple sclerosis in a pooled analysis of 2 randomized clinical trials. *JAMA Neurol*. 2020;77(9):1132-1140. doi:10.1001/jamaneurol.2020.1568
25. Elliott C, Wolinsky JS, Hauser SL, et al. Slowly expanding/evolving lesions as a magnetic resonance imaging marker of chronic active multiple sclerosis lesions. *Mult Scler*. 2019;25(14):1915-1925. doi:10.1177/1352458518814117
26. Preziosa P, Pagani E, Meani A, et al. Slowly expanding lesions predict 9-year multiple sclerosis disease progression. *Neurol Neuroimmunol Neuroinflamm*. 2022;9(2):e1139. doi:10.1212/NXI.0000000000001139
27. He A, Merkel B, Brown JWL, et al. Timing of high-efficacy therapy for multiple sclerosis: a retrospective observational cohort study. *Lancet Neurol*. 2020;19(4):307-316. doi:10.1016/S1474-4422(20)30067-3
28. Harding K, Williams O, Willis M, et al. Clinical outcomes of escalation vs early intensive disease-modifying therapy in patients with multiple sclerosis. *JAMA Neurol*. 2019;76(5):536-541. doi:10.1001/jamaneurol.2018.4905
29. Brown FS, Glasmacher SA, Kearns PKA, et al. Systematic review of prediction models in relapsing remitting multiple sclerosis. *PLoS One*. 2020;15(5):e0233575. doi:10.1371/journal.pone.0233575
30. Misicka E, Sept C, Briggs FBS. Predicting onset of secondary-progressive multiple sclerosis using genetic and non-genetic factors. *J Neurol*. 2020;267(8):2328-2339. doi:10.1007/s00415-020-09850-z
31. Brownlee WJ, Altmann DR, Prados F, et al. Early imaging predictors of long-term outcomes in relapse-onset multiple sclerosis. *Brain*. 2019;142(8):2276-2287. doi:10.1093/brain/awz156
32. Treaba CA, Granberg TE, Sormani MP, et al. Longitudinal characterization of cortical lesion development and evolution in multiple sclerosis with 7.0-T MRI. *Radiology*. 2019;291(3):740-749. doi:10.1148/radiol.2019181719
33. Bodini B, Poirion E, Tonietto M, et al. Individual mapping of innate immune cell activation is a candidate marker of patient-specific trajectories of worsening disability in multiple sclerosis. *J Nucl Med*. 2020;61(7):1043-1049. doi:10.2967/jnumed.119.231340
34. Datta G, Colasanti A, Kalk N, et al. ^{11}C-PBR28 and ^{18}F-PBR111 detect white matter inflammatory heterogeneity in multiple sclerosis. *J Nucl Med*. 2017;58(9):1477-1482. doi:10.2967/jnumed.116.187161
35. Banati RB, Newcombe J, Gunn RN, et al. The peripheral benzodiazepine binding site in the brain in multiple sclerosis: quantitative in vivo imaging of microglia as a measure of disease activity. *Brain*. 2000;123(Pt 11):2321-2337. doi:10.1093/brain/123.11.2321
36. Giannetti P, Politis M, Su P, et al. Microglia activation in multiple sclerosis black holes predicts outcome in progressive patients: an in vivo [(11)C](R)-PK11195-PET pilot study. *Neurobiol Dis*. 2014;65:203-210. doi:10.1016/j.nbd.2014.01.018

37. Nutma E, Gebro E, Marzin MC, et al. Activated microglia do not increase 18 kDa translocator protein (TSPO) expression in the multiple sclerosis brain. *Glia*. 2021; 69(10):2447-2458. doi:10.1002/glia.24052
38. Nutma E, Stephenson JA, Gorter RP, et al. A quantitative neuropathological assessment of translocator protein expression in multiple sclerosis. *Brain*. 2019;142(11): 3440-3455. doi:10.1093/brain/awz287
39. Harrison DM, Roy S, Oh J, et al. Association of cortical lesion burden on 7-T magnetic resonance imaging with cognition and disability in multiple sclerosis. *JAMA Neurol*. 2015;72(9):1004-1012. doi:10.1001/jamaneurol.2015.1241
40. Lip GY, Nieuwlaat R, Pisters R, Lane DA, Crijns HJ. Refining clinical risk stratification for predicting stroke and thromboembolism in atrial fibrillation using a novel risk factor-based approach: the Euro Heart Survey on Atrial Fibrillation. *Chest*. 2010; 137(2):263-272. doi:10.1378/chest.09-1584
41. Cummings J, Aisen P, Apostolova LG, Atri A, Salloway S, Weiner M. Aducanumab: appropriate use recommendations. *J Prev Alzheimers Dis*. 2021;8(4):398-410. doi:10.14283/jpad.2021.41
42. Kaunzner UW, Kang Y, Zhang S, et al. Quantitative susceptibility mapping identifies inflammation in a subset of chronic multiple sclerosis lesions. *Brain*. 2019;142(1): 133-145. doi:10.1093/brain/awy296

TSPO-Detectable Chronic Active Lesions Predict Disease Progression in Multiple Sclerosis

Eero Polvinen, Markus Matilainen, Marjo Nylund, et al.

Neurol Neuroimmunol Neuroinflamm 2023;10;
DOI 10.1212/NXI.0000000000200133